Journal of Power Sources 195 (2010) 5749–5760

Contents lists available at ScienceDirect

Journal of Power Sources

journal homepage: www.elsevier.com/locate/jpowsour

Steam reforming of heptane in a fluidized bed membrane reactor

Mohammad A. Rakib[a,*], John R. Grace[a], C. Jim Lim[a], Said S.E.H. Elnashaie[b]

[a] Department of Chemical and Biological Engineering, University of British Columbia, 2360 East Mall, Vancouver, BC, Canada V6T 1Z3
[b] College of Engineering, Misr University for Science and Technology, Distinguished District, 6th of October Province, Egypt

ARTICLE INFO

Article history:
Received 20 January 2010
Received in revised form 24 March 2010
Accepted 24 March 2010
Available online 31 March 2010

Keywords:
Hydrogen production
Heptane
Steam reforming
Membrane reactor
Fluidized bed reactor
Experiments

ABSTRACT

n-Heptane served as a model compound to study steam reforming of naphtha as an alternative feedstock to natural gas for production of pure hydrogen in a fluidized bed membrane reactor. Selective removal of hydrogen using $Pd_{77}Ag_{23}$ membrane panels shifted the equilibrium-limited reactions to greater conversion of the hydrocarbons and lower yields of methane, an intermediate product. Experiments were conducted with no membranes, with one membrane panel, and with six panels along the height of the reactor to understand the performance improvement due to hydrogen removal in a reactor where catalyst particles were fluidized. Results indicate that a fluidized bed membrane reactor (FBMR) can provide a compact reformer for pure hydrogen production from a liquid hydrocarbon feedstock at moderate temperatures (475–550 °C). Under the experimental conditions investigated, the maximum achieved yield of pure hydrogen was 14.7 moles of pure hydrogen per mole of heptane fed.

1. Introduction

1.1. Background

Hydrogen demand is increasing in the petrochemical and petroleum processing sectors [1–4] and for other industrial applications. It may also increase significantly in the energy and transportation sectors [5–8]. Being a carbon-free fuel, hydrogen can assist in mitigating global warming due to greenhouse gas emissions if CO_2 emissions can be minimized during hydrogen production [9].

About 48% of industrial hydrogen is produced from natural gas as feedstock [10], largely due to the widespread availability of natural gas, as well as having the highest hydrogen-to-carbon ratio. However, for onboard hydrogen generation for mobile applications, liquid hydrocarbons like gasoline, naphtha, kerosene or diesel are advantageous feedstocks [11,12], safely storable under ambient conditions, and with much higher volumetric energy density than natural gas [13]. Liquid feedstocks like naphtha are often used for hydrogen production when natural gas is not available, accounting for about 30% of hydrogen production [10,14]. In refineries, feedstock versatility for steam reformers would be a great advantage due to fluctuating demand and supply of different feedstocks [15].

Naphtha is the most common liquid hydrocarbon feedstock for hydrogen production. For steam reforming, low aromatic-content naphtha (LAN) is preferred. Recently, naphtha prices have been unstable due to fluctuations in oil prices. For places with access to both naphtha and natural gas, naphtha tends to be an unprofitable feedstock for hydrogen production during peaks, while being preferred during slumps. Many steam reforming facilities worldwide, especially in India and China, have installed pre-reformer units upstream of natural gas steam reformers to facilitate feedstock flexibility.

For steam reforming of higher hydrocarbons, the major reactions can be written:

Higher hydrocarbons steam reforming

$$C_nH_m + nH_2O \rightarrow nCO + \left(n + \frac{m}{2}\right) H_2 \quad \Delta H^\circ_{298} = 1108\ \text{kJ mol}^{-1} \quad \text{for } n = 7 \tag{1}$$

Methanation and methane steam reforming

$$CO + 3H_2 \rightleftarrows CH_4 + H_2O \quad \Delta H^\circ_{298} = -206\ \text{kJ mol}^{-1} \tag{2}$$

Water gas shift

$$CO + H_2O \rightleftarrows CO_2 + H_2 \quad \Delta H^\circ_{298} = -41\ \text{kJ mol}^{-1} \tag{3}$$

Methane overall steam reforming

$$CH_4 + 2H_2O \rightleftarrows CO_2 + 4H_2 \quad \Delta H^\circ_{298} = 165\ \text{kJ mol}^{-1} \tag{4}$$

* Corresponding author. Tel.: +1 604 827 3177; fax: +1 604 822 6003.
E-mail addresses: rakib@interchange.ubc.ca, rakibche@gmail.com, mrakib@chbe.ubc.ca (M.A. Rakib).

0378-7753/$ – see front matter © 2010 Elsevier B.V. All rights reserved.
doi:10.1016/j.jpowsour.2010.03.072

Nomenclature

A_P	membrane permeation area
E_{H_2}	activation energy for permeation
FBMR	fluidized bed membrane reactor
HTS	high-temperature shift
LTS	low-temperature shift
MTS	medium-temperature shift
P	FBMR pressure monitored in the freeboard
$P_{H_2,M}$	hydrogen partial pressure on the permeate side
$P_{H_2,R}$	hydrogen partial pressure on the reactor side
P_m	permeate side pressure
P_{M_0}	pre-exponential factor for permeation
Q_{H_2}	hydrogen diffusion flux through the membrane
ROG	reformer off-gas
SCR	steam-to-carbon molar ratio
T_{av}	bed average temperature (based on temperatures of the levels of the six membrane panels or dummies)
δ_{H_2}	thickness of the membrane

Summing Eq. (1) and n times Eq. (3) leads to

$$C_nH_m + 2nH_2O = nCO_2 + \left(2n + \frac{m}{2}\right) H_2$$

For $n = 7$ (i.e. n-heptane):

$$C_7H_{16} + 14H_2O = 7CO_2 + 22H_2 \quad (5)$$

Since, under industrial operating conditions, excess steam is always used to minimize catalyst deactivation, the maximum hydrogen yield is 22 moles per mole of heptane fed.

1.2. Catalyst issues in steam reforming of higher hydrocarbons

Commercial catalysts for steam reforming of hydrocarbons are generally based on Ni, dispersed on a refractory support, due to its high activity and low cost. Other possible candidates include Co, Pt, Pd, Ru and Rh, the order of specific activities of metals supported on alumina or magnesia being Rh, Ru > Ni, Pd, Pt > Re > Co [16]. Ni catalysts present major coking problems because of the formation, diffusion and dissolution of carbon.

Higher hydrocarbons show a greater tendency to form carbon on Ni than methane. Therefore, special catalyst formulations containing alkali or rare earths, or based on an active magnesia support, are required [17]. For higher hydrocarbons, there is potential for various forms of carbon formation [18–23].

A common technique to reduce carbon formation is to employ a higher steam-to-carbon ratio than required stoichiometrically, the excess increasing with the number of carbons in the hydrocarbon chain. For example, in industrial naphtha steam reforming, steam-to-carbon ratios of 4 to 6 are common [24–26] compared with ~3 for natural gas. However, a high steam-to-carbon ratio decreases the thermal efficiency of the process, and also leads to a larger reformer due to the higher volumetric gas flow rates. On the other hand, in addition to resulting in higher rates of carbon formation, lower steam-to-carbon ratios also lead to higher methane leaving the reformer, which must then be compensated by maintaining a higher exit temperature. Intensive research on catalyst design is being carried out to decrease this ratio [27].

1.3. Naphtha steam reforming: industrial practice

1.3.1. Conventional naphtha steam reforming

Since steam reforming of methane is endothermic and equilibrium-limited, industrial natural gas steam reformers operate at temperatures >850 °C to achieve high conversions. However, the same operating conditions cannot be applied to higher hydrocarbon feedstocks like naphtha because such high temperatures would cause rapid catalyst deactivation due to carbon formation and shorter reformer tube life. A conventional naphtha steam reformer uses catalysts promoted with alkali compounds to suppress carbon formation [28]. In many cases, two catalysts are provided, with the entrance of the reformer loaded with a more robust catalyst to handle heavier feeds. A high steam-to-carbon ratio, usually >4.0, is used to suppress catalyst deactivation [29,30]. A lower average operating temperature is employed, with typical inlet and outlet temperatures of 485 and 850 °C, respectively. Commercially available naphtha steam reforming catalysts have nickel loadings from 15% to ~25%, most again promoted by K_2O.

1.3.2. Steam reforming with pre-reformer

A modern hydrogen plant accepting naphtha feedstock starts with an additional unit, the pre-reformer, after feed desulfurization. Pre-reforming of the desulfurized hydrocarbon feedstock makes the gas feed to the primary reformer practically free of higher hydrocarbons, which are converted directly to C_1 components with no intermediate hydrocarbon products. Thus, while the pre-reformer operates with specially designed pre-reformer catalysts at temperatures from 450 to 550 °C [23,29], the methane-rich gas from the pre-reformer can be heated to >650 °C before entering the reformer operating at exit temperatures of ~950 °C [29]. Industrial pre-reformer catalysts are typically highly Ni-loaded, ~25–30% (by weight) for pre-reforming of lighter hydrocarbons up to LPG, and >50% for the naphtha range. The catalysts are characterized by high resistance to sulfur-poisoning and coke formation. At the practiced pre-reforming temperatures, undesired reactions like pyrolysis, steam cracking of higher hydrocarbons, and polymerization of alkenes are minimal. All forms of carbon formation can be avoided by properly choosing the temperature window for steam reforming [23,28]. The higher hydrocarbon steam reforming reactions are practically irreversible, and thus the hydrogen yields are limited by the equilibrium of the methane steam reforming reactions. Downstream of the pre-reformer, the steam reformer therefore tends to operate at typical methane steam reforming operating conditions, and utilize regular methane steam reforming catalysts.

The first naphtha steam reformer dates back to 1962 at ICI, with an operating pressure of 15 bars [28,31,32]. Some naphtha steam reformers have been operated at low temperatures to produce a methane-rich substitute natural gas. A Topsoe naphtha steam reformer was introduced in 1965, and a pre-reformer was first installed by Topsoe in 1986 [31]. Fig. 1 shows the block diagram of a modern higher hydrocarbon steam reforming set-up incorporating a pre-reformer. Pre-reforming catalysts have high nickel loadings, typically in excess of 25% by weight and some as high as 55%.

In the process for making hydrogen, the synthesis gas mixture leaving the steam reformer has few downstream units to purify the hydrogen. Traditionally, the shift conversion reaction following the reformer used to be conducted in two stages: a high-temperature shift (HTS) converter followed by a low-temperature shift (LTS) converter. With more recent steam reforming plants operating at low steam-to-carbon ratios, these reactors are replaced by a single medium-temperature shift (MTS) converter. A CO_2 removal section and a methanator (to remove CO traces) may follow the shift conversion. Recent developments also have CO_2 removal and methanation units replaced by pressure swing adsorption (PSA) to produce hydrogen of purity up to 99.999% [33].

1.3.3. Fluidized bed membrane reformer (FBMR)

Fine catalyst particles ideal for fluidization increase the catalyst effectiveness factor from as low as 0.01–0.001 in fixed bed reform-

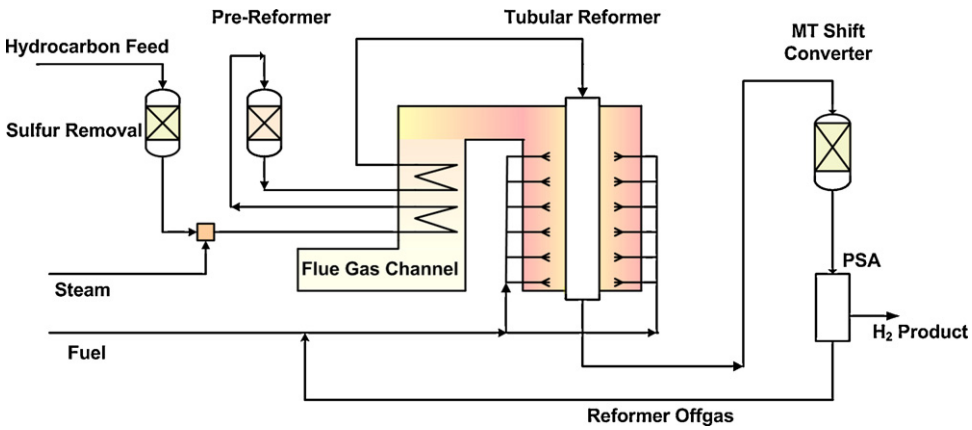

Fig. 1. Key components in a modern steam reforming plant for hydrogen from higher hydrocarbon feedstock (adapted from Rostrup-Nielsen and Rostrup-Nielsen [1]).

ers to almost unity [34,35]. Better thermal uniformity in a fluidized bed can prevent hotspots. Selective removal of hydrogen from the reaction environment via permselective Pd alloy membranes drives the equilibrium methane steam reforming and water gas shift conversions forward, thereby significantly enhancing the hydrogen yield [36–39]. The fluidized bed and membrane reactor concepts developed at the University of British Columbia [40,41], has been commercialized by Membrane Reactor Technologies [42]. Rakib et al. [43] provided a FBMR model for steam reforming of heptane, and predicted that an FBMR for higher hydrocarbons can result in a compact reformer system, combining pre-reforming, reforming and hydrogen purification in a single unit. This paper focuses on the technical feasibility of such a reformer unit, with n-heptane as a surrogate for naphtha, as in some previous studies [23,43–47].

1.4. Thermodynamics of n-heptane steam reforming

A HYSYS steady-state simulator was first used to examine the thermodynamics of heptane steam reforming for operating conditions spanning the experimental conditions. Fig. 2 shows the dry gas compositions at a steam-to-carbon molar ratio of 5 for pressures of 400 and 800 kPa. Fig. 3 shows dry gas compositions at a pressure of 400 kPa and steam-to-carbon molar ratios of 4 and 6. It is seen that heptane is fully consumed, indicating that heptane reforming is essentially irreversible for temperatures from 400 to 800 °C. Irreversibility of steam reforming is a general feature for higher hydrocarbons having different degrees of reactivity [28]. Industrial steam reforming of light gas oils and diesel fuels produces syngas with no traces of higher hydrocarbons in the product [1]. Equilibrium predictions also show the absence of intermediate hydrocarbons other than methane, except for a trace of ethane (~0.1% typically).

Hydrogen production increases as temperature is increased, decreasing the equilibrium content of methane. This is because the steam reforming of methane is endothermic. Also, since the reactions involve a net increase in molar flow, Le Chatelier's principle requires that increasing pressure decreases the hydrogen production, as is evident from Fig. 2. Higher steam partial pressure has a positive effect on hydrogen production, as seen in Fig. 3.

2. FBMR for steam reforming of heptane

2.1. FBMR experimental set-up

An FBMR pressure vessel, shown in Fig. 4, was fabricated to allow experiments up to 10 barg and 621 °C. A commercial naphtha steam reforming catalyst, RK-212 from Haldor Topsoe A/S, was crushed and sieved to a Sauter mean particle diameter of 179 μm. Pd membranes are infinitely selective to hydrogen permeation due to the unique solution-diffusion mechanism of permeation [48,49]. Hydrogen diffusion flux depends on the difference between the square roots of partial pressures on the two sides according to Sieverts law, with diffusion as the rate-determining step [50]:

$$Q_{H_2} = A_p \frac{P_{M_0}}{\delta_{H_2}} \exp\left(\frac{-E_{H_2}}{RT}\right)\left(\sqrt{P_{H_2,R}} - \sqrt{P_{H_2,M}}\right) \quad (6)$$

Pd is often alloyed with other metals like Ag, Cu and Ru to improve mechanical stability, resistance to hydrogen embrittlement and hydrogen permeation flux. In our study, double-sided membrane panels, manufactured by Membrane Reactor Technologies [51] with a 25 μm thick $Pd_{77}Ag_{23}$ alloy foil layer, were inserted through six alternately arranged vertical slots on the wall

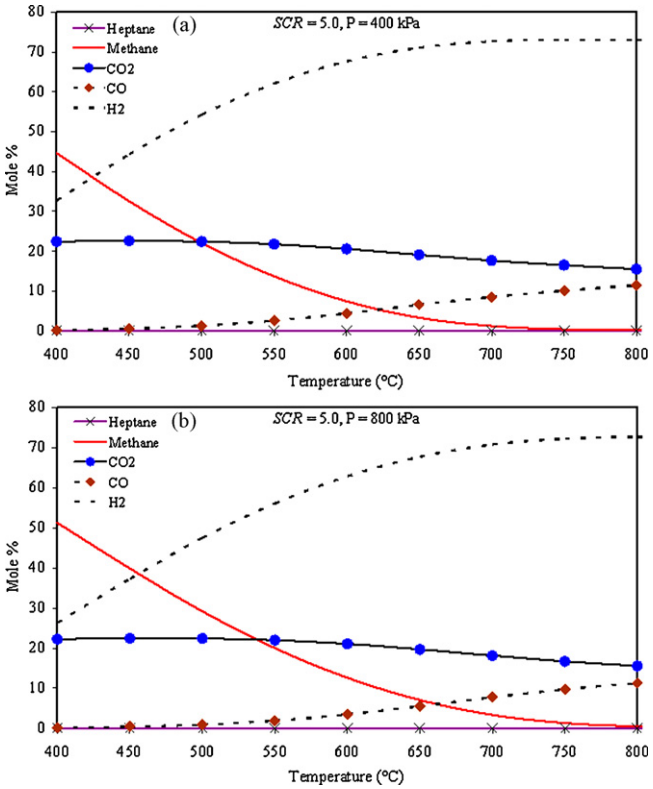

Fig. 2. Dry gas equilibrium composition for steam-to-carbon molar ratio of 5.0: (a) P = 400 kPa and (b) P = 800 kPa. No membranes present.

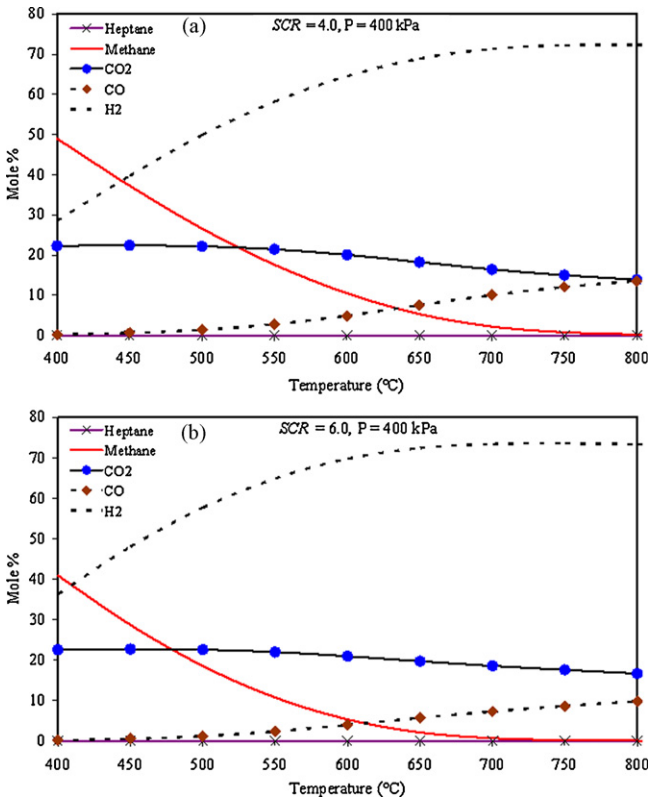

Fig. 3. Dry gas composition for reactor pressure of 400 kPa: (a) steam-to-carbon molar ratio = 4.0 and (b) steam-to-carbon molar ratio = 6.0. No membranes present.

of the reactor. These panels, shown schematically in Fig. 5(a), are 231.8 mm × 73.0 mm × 6.35 mm thick. Accounting for welding and bonding space, the active area of each membrane is 206.4 mm × 50.8 mm on each side of the membrane panels to withdraw hydrogen along the reactor height. High-purity hydrogen, metered by mass flow meters, FMA-1818 from Omega Instruments, passed through the membrane panels to a spark-proof hydrogen

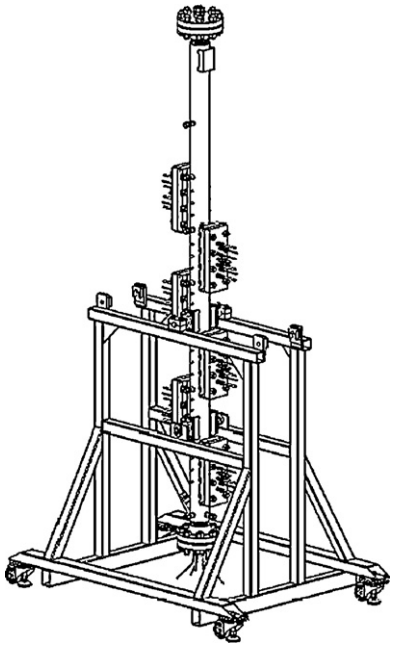

Fig. 4. Drawing of FBMR pressure vessel supported on mobile stand.

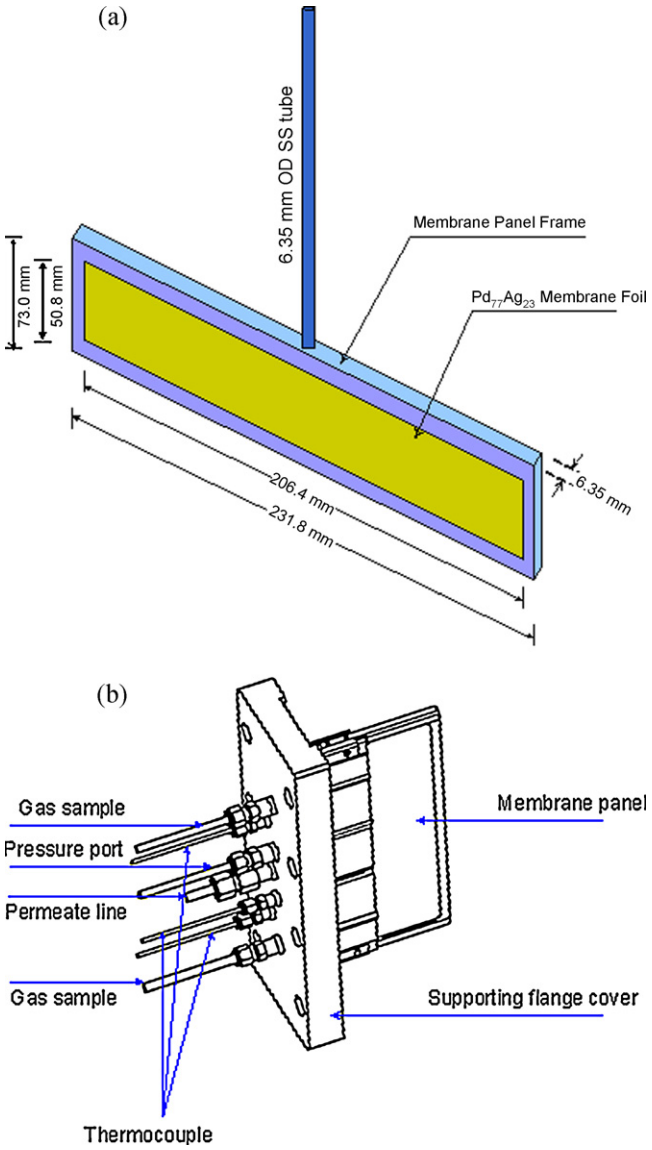

Fig. 5. (a) Dimensions of membrane panel. (b) Ports arranged on each side-opening cover where membrane panels are installed.

vacuum pump. In some experiments, stainless steel dummies of the same dimensions as the active membrane panels were installed, as explained below. Fig. 5(b) shows a membrane panel installed onto a supporting side flange cover.

Fig. 6 depicts the experimental set-up. Before starting the experiments, the catalyst was reduced overnight at about 500 °C. The required steady flow rate of steam was established before feeding heptane. The vapor head-space in the heptane storage tank was pressurized by helium, pushing the heptane through a liquid heptane Bronkhorst mass flow controller. Distilled water was pumped, metered by a Brooks mass flow controller, and flowed through an electrically heated vaporizer. Heptane was mixed with the steam downstream of the vaporizer. The heptane/steam mixture was fed to the FBMR through a doughnut-shaped gas distributor, located inside and at the bottom of the FBMR, with six equally spaced holes drilled on the inner side. This allowed spent catalysts to be discharged through a catalyst drain in the bottom head cover, without completely disassembling the bottom head. The steam-to-carbon ratio in the feed was maintained by adjusting the mass flow rates of water and heptane.

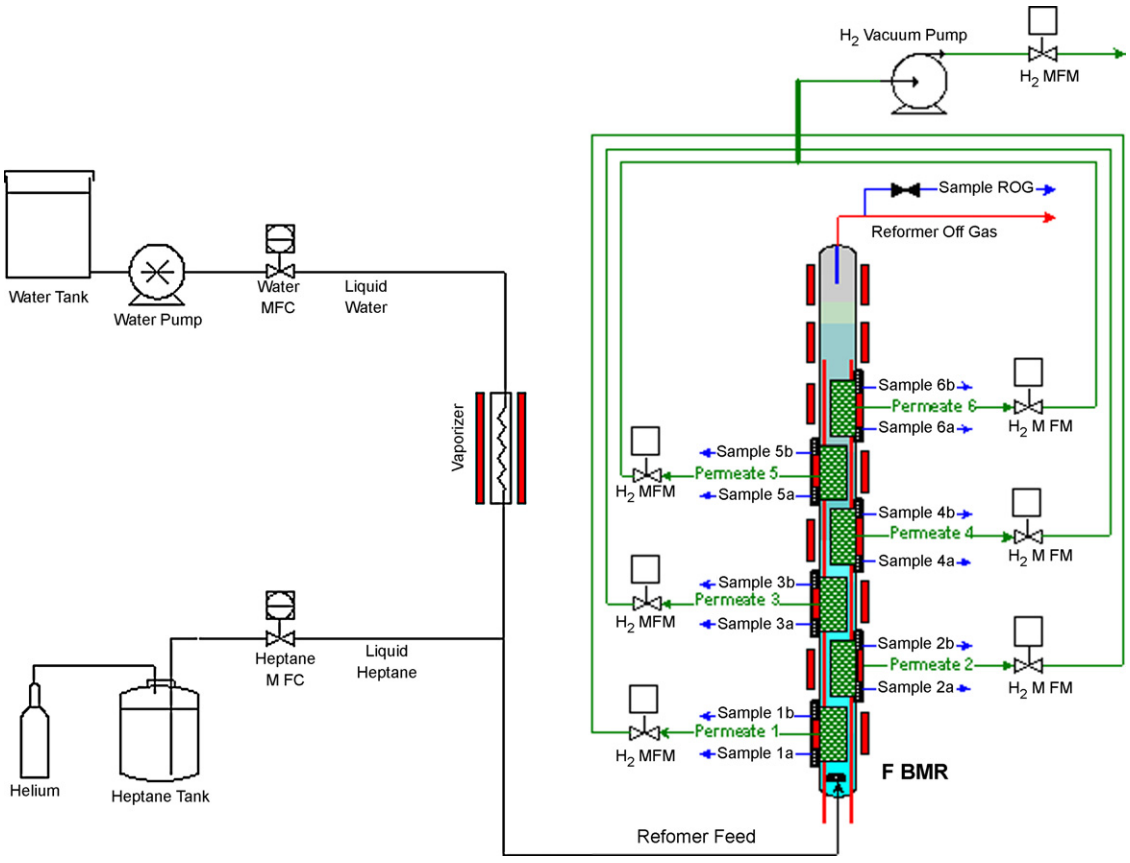

Fig. 6. Schematic of experimental set-up to study steam reforming of n-heptane.

2.2. Experimental plan and performance characterization

Table 1 summarizes the steady reactor measurements made to characterize the reactor performance. Table 2 lists the location of the monitoring probes, and the location and height intervals covered by the membrane panels. The reactor performance was characterized by measuring the pure hydrogen produced and the gas compositions at different locations. The composition of the gas samples was analyzed by a Varian micro-GC CP-4900 (see Table 3). Table 4 gives key details of the experiments on the steam reforming of heptane. A steam-to-carbon ratio (SCR) of 5 was used for all experiments, except when SCR itself was a parameter. While most of these experiments maintained similar feed superficial velocities for parametric studies, some provided similar molar feeds. These experiments were conducted in three phases: Sets 1–3 were carried out with six membrane dummies, set 4 with five dummies and one active membrane panel (at the 5th side opening from the bottom), and sets 5–9 with six active membranes installed. The fluidized bed reactor without membranes is comparable to a pre-reformer without removal of hydrogen. Experiments with one and six membrane panels help to elucidate the effect of hydrogen removal on the reactions inside the reactor.

Steam reforming of higher hydrocarbons is very rapid, and the conversion of the higher hydrocarbons is irreversible, limited only by equilibrium of methane steam reforming. Thus, conversion of the higher hydrocarbon fed becomes irrelevant, being essentially 100% from near the entrance of industrial set-ups [23], and also for an FBMR with heptane feed [43,52]. Since the objective is to produce pure hydrogen, pure hydrogen yield is the most relevant performance metric. To compare the reformer with and without membranes, the total hydrogen yield, including both permeated pure and retentate hydrogen, is calculated and plotted. The yield of carbon oxides, especially carbon dioxide, is an equivalent measure to describe the conversion of the hydrocarbons, including the intermediate. Carbon dioxide is a co-product from reactions (3) to (5). Based on the dry composition of gas samples withdrawn from the FBMR at different heights, local yields of retentate hydrogen, carbon oxides and methane are calculated:

$$\text{Pure hydrogen yield} = \frac{\text{molar flow of pure hydrogen extracted via membranes}}{\text{molar heptane feed rate}} \tag{7}$$

$$\text{Retentate hydrogen yield} = \frac{\text{molar flow of hydrogen in retentate stream}}{\text{molar heptane feed rate}} \tag{8}$$

$$\text{Total hydrogen yield} = \text{pure hydrogen yield} + \text{retentate hydrogen yield} \tag{9}$$

$$\text{Carbon oxides yield} = \frac{(\text{molar flow of CO} + \text{molar flow of } CO_2) \text{ in retentate stream}}{7 \times \text{molar heptane feed rate}} \tag{10}$$

$$\text{Methane yield} = \frac{\text{molar flow of methane in retentate stream}}{7 \times \text{molar heptane feed rate}} \tag{11}$$

Table 1
Steady-state reactor measurements.

Quantity	Device and location
FBMR temperatures	One thermocouple just above distributor. One thermocouple close to center of each membrane panel. One thermocouple for freeboard just upstream of reformer exit.
Gas composition	Two sampling ports for each of the six lateral flanges supporting a membrane panel. One sampling line for ROG. Gas sampled from these sampling points are analyzed online by a Varian micro-GC CP-4900 using sample selection valves.
Permeate hydrogen production	Flow rates of permeate hydrogen from each membrane panel are measured using FMA-1818 mass flow meters from Omega Instruments.
Purity of permeate hydrogen	Hydrogen purity in permeate product from each membrane panel are analyzed by the micro-GC.
Pressures	Absolute pressures in the feed line, freeboard, and at the distributor level in bed are determined using PX-309 absolute pressure transducers from Omega Instruments. Differential pressure between alternate levels of side flanges (i.e. pairs 1–3, 3–5, 2–4, and 4–6) and between distributor and freeboard are measured using PX-2300 differential pressure transducers from Omega Instruments.

Table 2
Location of sampling ports, thermocouples and pure hydrogen withdrawal, and height intervals of active membrane surface.

Description (side opening counted from bottom)	Location above distributor holes (m)	Height interval covered by active membrane
Thermocouple (bottom)	0.01	–
Thermocouple (side opening 1)	0.32	–
Thermocouple (side opening 2)	0.52	–
Thermocouple (side opening 3)	0.78	–
Thermocouple (side opening 4)	1.08	–
Thermocouple (side opening 5)	1.29	–
Thermocouple (side opening 6)	1.59	–
Thermocouple (freeboard)	2.33	–
Gas samples (side opening 1)	0.22, 0.37	–
Gas samples (side opening 2)	0.47, 0.63	–
Gas samples (side opening 3)	0.73, 0.88	–
Gas samples (side opening 4)	0.98, 1.13	–
Gas samples (side opening 5)	1.24, 1.39	–
Gas samples (side opening 6)	1.49, 1.64	–
Pure hydrogen (side opening 1)	0.30	0.19–0.40
Pure hydrogen (side opening 2)	0.55	0.45–0.65
Pure hydrogen (side opening 3)	0.80	0.70–0.91
Pure hydrogen (side opening 4)	1.06	0.95–1.16
Pure hydrogen (side opening 5)	1.31	1.21–1.41
Pure hydrogen (side opening 6)	1.57	1.46–1.67

3. Results and discussion

3.1. FBMR experiments

In most experiments, two or three samples were analyzed at each location. Error bars, corresponding to the standard deviations ($\pm\sigma$) for each sample gas location, are plotted below with some data points shifted very slightly sideways to allow clear display.

For each membrane panel there is one thermocouple close to the hydrogen removal port. An average bed temperature was calculated based on the temperatures recorded at all six membrane levels. For each parametric study, the time-average bed temperature was kept constant, except where the average bed temperature was itself the study parameter. Gas samples were withdrawn from two levels for each side opening. A spline interpolation method function was used to estimate the temperatures corresponding to these sampling port levels. For each parametric study, fitted temperature profiles are plotted with profiles of the carbon oxides yield, methane yield, and hydrogen yield. The heptane conversion exceeded 99% at the lowest sampling point, and was 100% for all samples above that. Hence, heptane conversion is not plotted here. For cases with one or more membranes present, the pure hydrogen and total hydrogen yields are plotted. The retentate hydrogen can be estimated from the difference between these two values.

3.2. Influence of key operating parameters

Fig. 7 depicts the performance of heptane steam reforming with no in-situ hydrogen removal, representing experiments 1.a and 1.b in Table 4. Higher temperature is seen to favour the steam reforming of methane. This is also accompanied by a higher hydrogen and carbon oxides yield by favouring reaction (2) in the backward, and (3) and (4) in the forward, direction. Carbon dioxide was the major carbon oxide, with carbon monoxide only ~1% of the dry gas.

Fig. 8 examines the influence of reactor pressure by comparing results for experiments 2 and 1.a with identical total molar

Table 3
Micro-GC column information for product gas analysis.

Channel	Column description	Carrier gas	Gases analyzed	Detection limits
1	10 m mol sieve 5A with pre-column backflush	Argon	He, H_2, O_2, N_2, CH_4 and CO	10–100 ppm
2	10 m PPU with pre-column backflush	Helium	CO_2, C_2H_4, C_2H_6, C_2H_2, H_2S and COS	10–100 ppm
3	8 m Silica PLOT with pre-column backflush	Helium	C_3 and C_4 isomers	10–100 ppm
4	8 m CP-Sil 5 with no pre-column	Helium	C_5–C_{12} components	1–10 ppm

Table 4
Experimental runs for steam reforming of n-heptane.

Expt no.	Active membranes (location)	Total feed rate (mol min^{-1})	T_{av} (°C)	P (kPa)	P_m (kPa)	SCR
1.a	None	0.673	520	460	NA	5.0
1.b		0.766	450	460	NA	5.0
2	None	0.673	520	725	NA	5.0
3.a	None	0.673	520	725	NA	4.0
3.b		0.673	520	725	NA	6.0
4.a	1 (#5)	0.717	480	585	101	5.0
4.b		0.717	480	585	35	5.0
4.c		0.717	480	720	101	5.0
4.d		0.717	480	720	26	5.0
5.a	6 (#1–#6)	0.635	475	600	25	5.0
5.b		0.614	500	600	25	5.0
5.c		0.595	525	600	25	5.0
6.a	6 (#1–#6)	0.410	500	400	25	5.0
6.b		0.819	500	800	25	5.0
7.a	6 (#1–#6)	0.635	475	600	101	5.0
7.b		0.635	475	600	50	5.0
8.a	6 (#1–#6)	0.614	500	600	25	4.0
8.b		0.614	500	600	25	6.0
9	6 (#1–#6)	0.819	500	600	25	5.0

feed rates and average temperature. The experimental hydrogen yield was higher at the lower pressure of 460 kPa, as expected from thermodynamics. Correspondingly, the yield of carbon oxides was found to be higher, and of methane lower, for 460 kPa than for 725 kPa. This indicates that the experiments were thermodynamically, rather than, kinetically, controlled.

Fig. 9 plots information from experiments 2, 3.a, and 3.b to show the effect of varying the steam-to-carbon molar ratio (SCR), with the same total molar feed rates. In the range of operation of these experiments, increasing steam partial pressure positively affected the conversion of the intermediate component methane, resulting in a lower methane yield. This also gave higher yields of hydrogen and carbon oxides. Higher SCR also enhanced gasification of any deposited carbon, thereby reducing catalyst deactivation. However, for the maximum possible hydrogen yield (see Eq. (5)), an SCR of 2 is required. Thus, a higher SCR is likely to decrease the energy efficiency of the process due to the energy required to raise excess steam.

Fig. 10 plots the experimental hydrogen yield against the thermodynamic equilibrium values computed corresponding to the

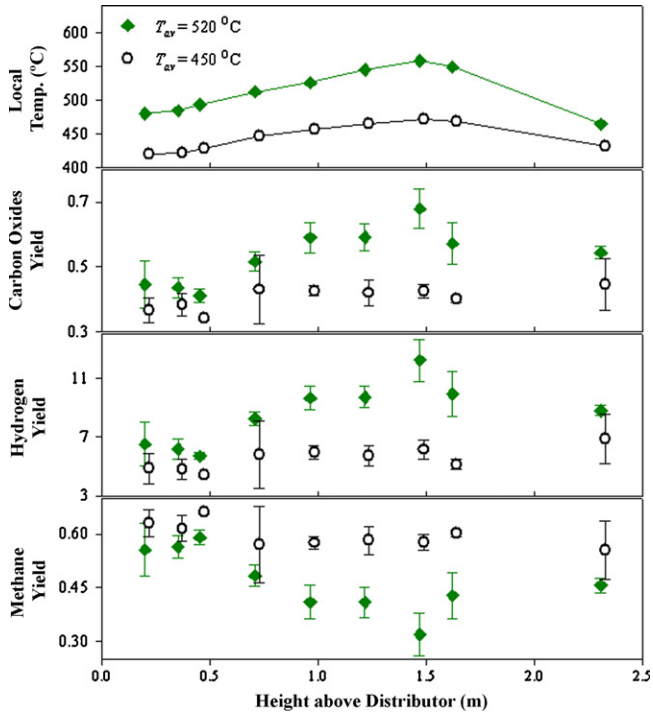

Fig. 7. Experimental yields and temperature for heptane steam reforming without active membrane panels at reactor pressure of 470 kPa and steam-to-carbon ratio molar ratio of 5.0. Total reactor feed = 0.673 and 0.766 mol min^{-1} at 520 and 450 °C, respectively.

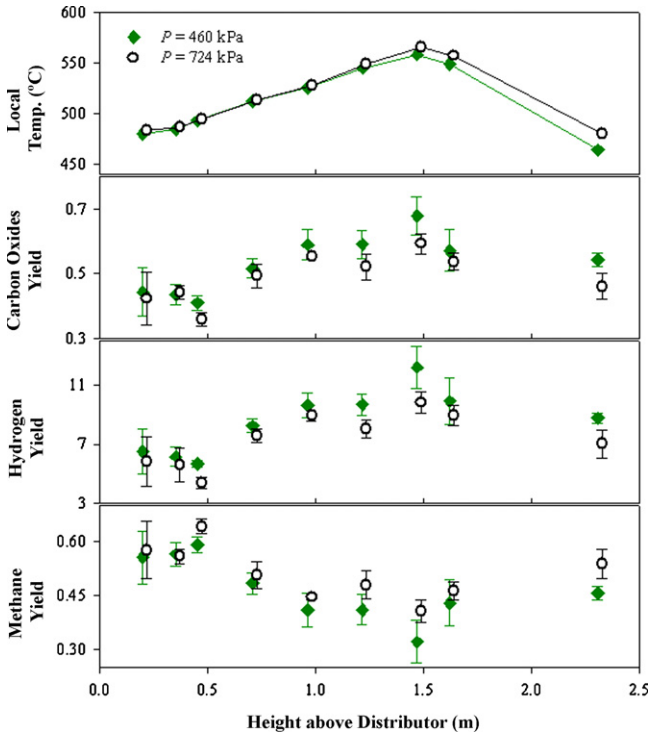

Fig. 8. Experimental yields and temperature for heptane steam reforming without active membrane panels at average reactor temperature of 520 °C and steam-to-carbon ratio molar ratio of 5.0. Total reactor feed = 0.673 mol min^{-1}.

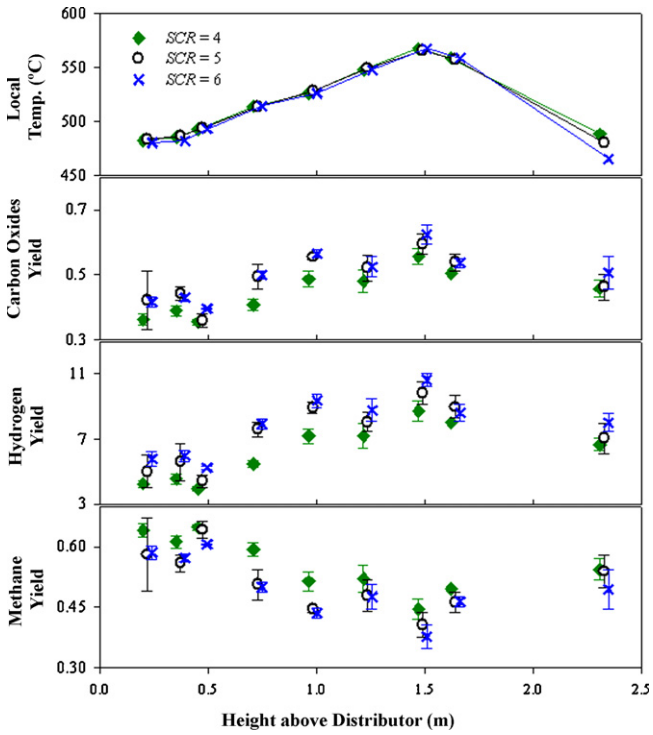

Fig. 9. Experimental yields and temperature for heptane steam reforming without active membrane panels at average reactor temperature of 520 °C and reactor pressure of 725 kPa. Total reactor feed = 0.673 mol min^{-1}.

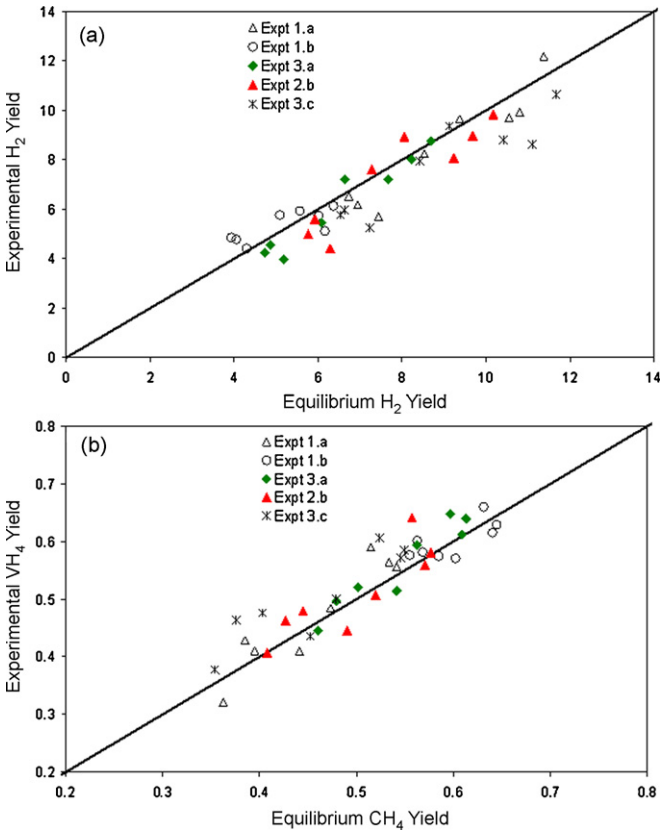

Fig. 10. Parity plot of experimental yields without active membrane panels against local equilibrium values: (a) hydrogen yield and (b) methane yield.

local temperatures for experiment sets 1–3. The experimental data closely follow the equilibrium values, indicating that the reactor without membranes is controlled by thermodynamic equilibrium.

Fig. 11 corresponds to experiments 4.a through 4.d, where only one active membrane panel was installed with the active membrane length spanning from 1.21 to 1.41 m above the distributor. The shaded band in this figure denotes the zone where pure hydrogen is removed by the membrane. For structural similarity among all experiments, dimensionally identical stainless steel dummy plates were installed in the other five openings. Two reactor pressures were studied, with and without suction on the membrane permeation side for each level. The total molar feed rate was the same for these four runs, with identical average reactor temperatures, so that experiments 4.a and 4.b had lower residence times than 4.c and 4.d. It is seen that experiments 4.a and 4.c had similar performance. This is due to the higher driving force and higher residence time available for hydrogen permeation for 4.c, compared to 4.a, counteracted by a negative impact of the thermodynamic equilibrium for the higher reactor pressure of 4.c. This also applies to similar performance exhibited by 4.b and 4.d for the permeate side operated under vacuum (35 and 26 kPa, respectively). The two runs with evacuated permeate (4.b and 4.d) showed better performances than without vacuum (4.a and 4.c). Note that the difference between these two pairs of runs became prominent after reaching the 5th flange where the single membrane panel was installed.

Figs. 12–16 correspond to experiment sets 5–9, each conducted with six active membrane panels along the reactor. The shaded bands in these figures represent intervals where pure hydrogen was withdrawn by membrane panels.

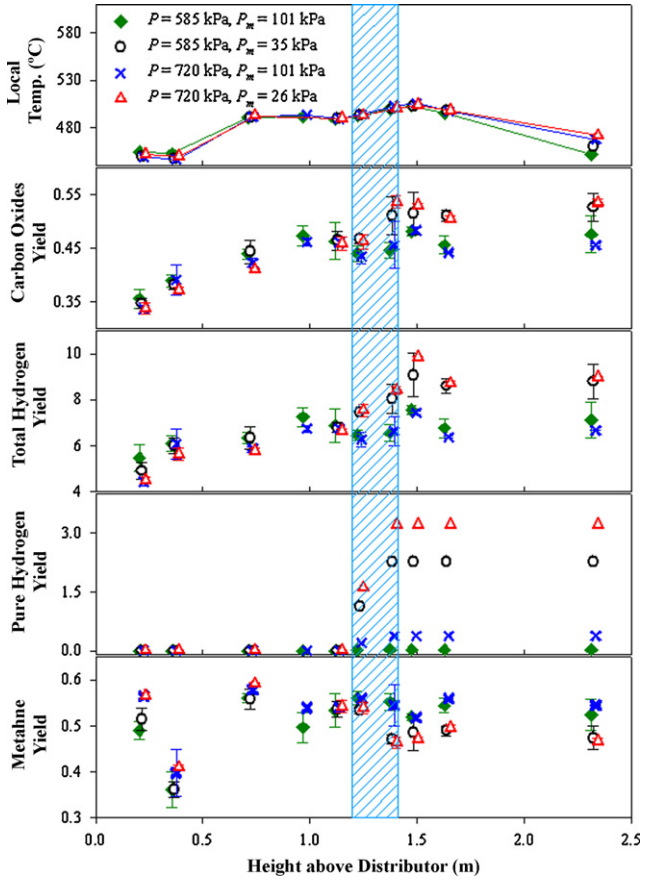

Fig. 11. Experimental yields and temperature for heptane steam reforming at average reactor temperature of 480 °C and steam-to-carbon molar ratio 5.0. One membrane panel installed, spanning from 0.95 to 1.16 m above distributor. Total reactor feed = 0.717 mol min^{-1}.

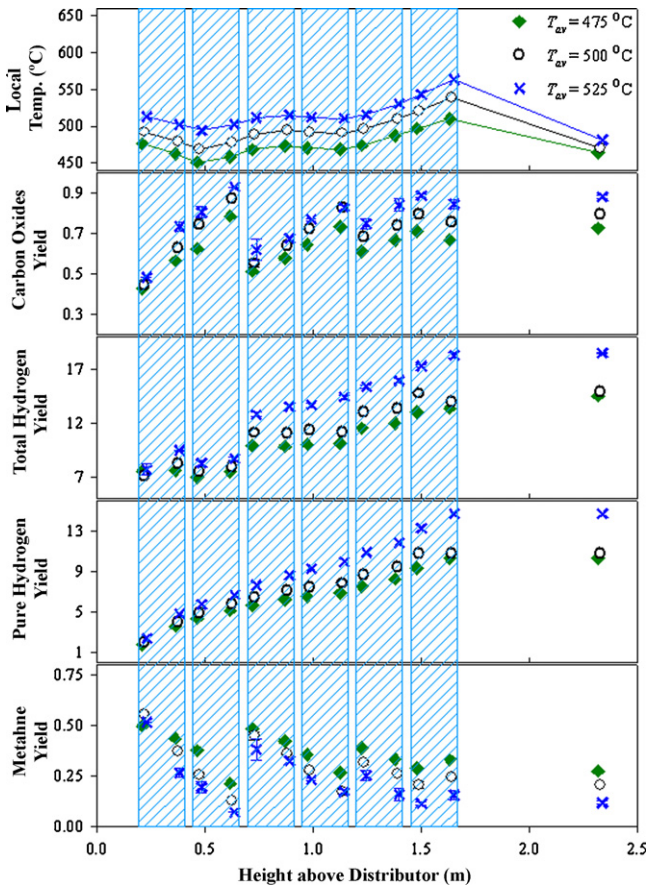

Fig. 12. Experimental yields and temperature for heptane steam reforming at pressure of 600 kPa, permeate pressure 25 kPa, and steam-to-carbon molar ratio 5.0. Six membrane panels installed. Total reactor feeds = 0.635, 0.614, and 0.595 mol min^{-1} for 475, 500, and 525 °C, respectively.

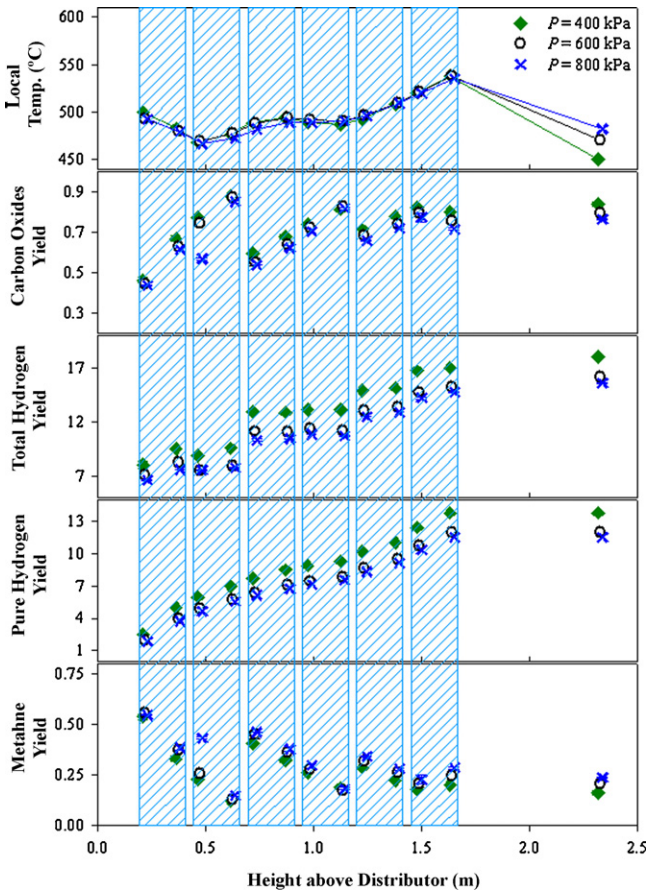

Fig. 13. Experimental yields and temperature for heptane steam reforming at average reactor temperature of 500 °C, permeate pressure 25 kPa, and steam-to-carbon molar ratio 5.0. Six membrane panels installed. Total reactor feeds = 0.410, 0.614, and 0.819 mol min^{-1} for P = 400, 600, and 800 kPa, respectively.

Fig. 12 presents the effect of reactor temperature, with increments of 25 °C in the average reactor temperature. The most important reactions (reactions (1)–(4) as listed) are endothermic on an overall basis, with only the water gas shift reaction (Eq. (3)) exothermic. In addition to the effect on equilibrium, an increase in membrane temperature increases hydrogen permeation (Eq. (6)), shifting the reversible reactions in the forward direction. This is reflected in the higher yield of permeate hydrogen, contributing to the greater total hydrogen yield as the average reactor temperature increased. The methane yield decreased due to higher consumption of methane (Eq. (4)). These trends are reflected in increased yield of carbon oxides.

Fig. 13 portrays the effect of the reactor pressure (400, 600 and 800 kPa), with the average bed temperature maintained at 500 °C. To keep the superficial gas velocities similar for all three pressures, the feed total molar flow rates were adjusted. The permeate side pressure was 25 kPa for all three cases, set by modulating the speed of the hydrogen vacuum pump. The total hydrogen yield decreased significantly when the pressure increased from 400 to 600 kPa, but a further increase from 600 to 800 kPa affected the hydrogen yield only marginally. Increased pressures negatively affect the equilibrium of the system, while also causing more hydrogen permeation flux due to increased pressure difference between the reactor and permeate sides. The thermodynamic effect is dominant at lower reactor pressures, but not at higher reactor pressures. This substantiates the fact that the fast kinetics of the steam reforming reactions make the system reach local equilibrium rapidly so that the performance is limited by the membrane permeation capacity.

Fig. 14 investigates the effect of the permeate side pressure with the reactor pressure and average bed temperature fixed at 600 kPa and 475 °C, respectively. The feed flow rates were the same for runs 5.a, 7.a and 7.b. Little hydrogen permeated through the membranes when the permeate side was at ambient pressure (vacuum pump not operated). The hydrogen permeation rate jumped significantly when the permeate side was evacuated to 50 kPa or 25 kPa, reflected in increases in total hydrogen yield and carbon oxides yield, and a decreasing methane yield, with greater removal of hydrogen from the reactor. In these experiments, the feed steam-to-carbon molar ratio was 5.0, while stoichiometrically only 2 is required (Eq. (5)). As a result, the bulk of the reactor gas stream consists of steam, and a higher reactor pressure does not necessarily translate to higher hydrogen partial pressure inside the reactor. When the permeate side pressure was atmospheric, the local partial pressure of hydrogen on the reactor side was estimated to be between 60 and 90 kPa, depending on the local conditions, with an average of 76 kPa. Thus, there was no driving force to promote hydrogen permeation through the membranes, and no hydrogen permeation was recorded. The average local hydrogen partial pressures were estimated to have been 67 kPa for P_m = 50 kPa, and 59 kPa for P_m = 25 kPa. Accordingly, hydrogen then permeated through the membranes, due to the positive driving force.

Fig. 15 shows the effect of the steam-to-carbon molar ratio (SCR). As for the experiments with no hydrogen removal, higher steam partial pressure positively influenced the hydrogen yield. A similar effect is also seen with the six membranes installed. More

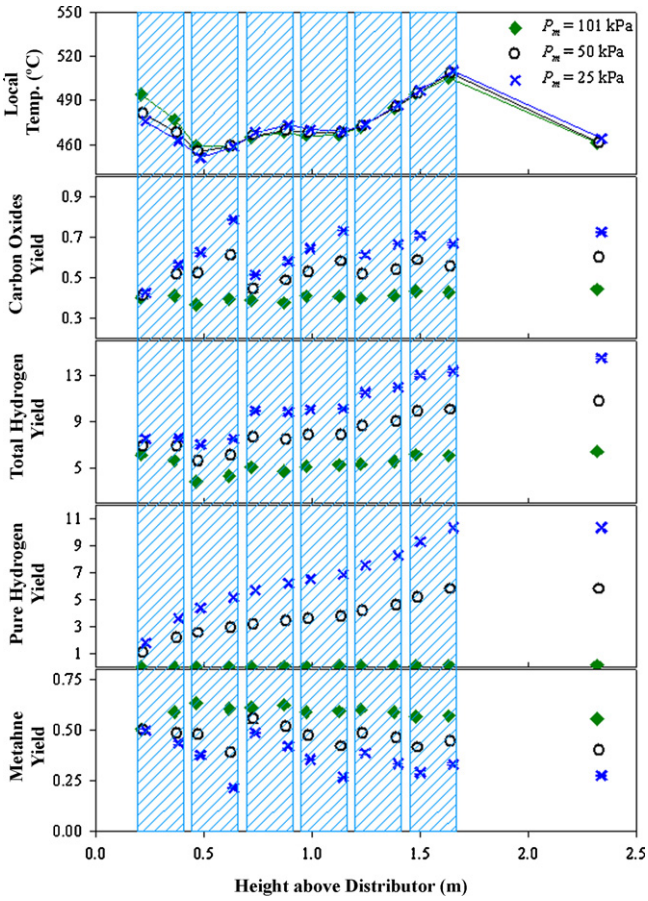

Fig. 14. Experimental yields and temperature for heptane steam reforming at average reactor temperature of 475 °C, pressure 600 kPa, and steam-to-carbon molar ratio 5.0. Six membrane panels installed. Total reactor feed = 0.635 mol min^{-1}.

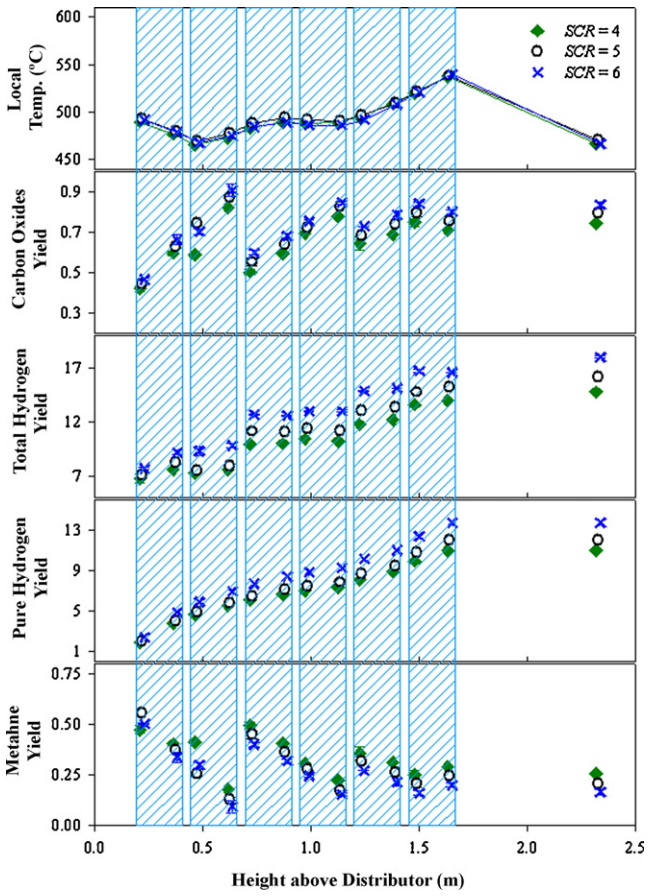

Fig. 15. Experimental yields and temperature for heptane steam reforming at average reactor temperature of 500 °C, pressure 600 kPa, and permeate pressure 25 kPa. Six membrane panels installed. Total reactor feed = 0.614 mol min^{-1}.

methane was consumed, reflected in the dwindling methane yield with increasing SCR.

Fig. 16 investigates the effect of superficial velocity. Gas superficial velocities increase as a result of the increasing molar flow provided by the steam reforming reactions, but decrease when hydrogen is removed from the system through the membranes. They are also affected by local temperature and pressure. Hence, the influence is described in terms of the feed molar flow rates, instead of the superficial velocity. Other operating conditions like average bed temperature, reactor pressure, permeate pressure and SCR were maintained constant for the two cases (5.b and 9) compared. Performance profiles are seen to differ near the entrance of the reactor, suggesting different hydrodynamic behaviour near the entrance. However, beyond the entrance region, the performance shows only marginal differences, indicating that the overall reactor performance was dominated by the reaction equilibria.

In Fig. 17, experimental hydrogen and methane yields are plotted against the corresponding equilibrium values at local temperatures without hydrogen removal. The experimental data were obtained 1.64 m above the distributor, i.e. at the top of the sixth membrane panel. With no hydrogen removal corresponding to experiment sets 1–3, hydrogen yield was close to, but less than the equilibrium value, whereas methane slip was more than predicted by equilibrium. For the permeate side operating at ambient pressure, the performance did not improve much relative to cases without membranes, regardless of whether only one membrane or all six were installed. As expected, there was a significant improvement in the hydrogen and methane yields with six membranes compared with one, demonstrating that the reactor performance was dominated by the available membrane permeation area, as well as by the permeate side pressure.

The carbon oxides and methane yields generally follow the temperature profile along the length of the reactor, since the gas composition in the reactor is governed by the local thermodynamic equilibrium. This has been observed for most of the sampling points along the reactor length. For each membrane interval, the effect of hydrogen permeation was apparent, with a higher carbon oxides yield and a lower methane yield at the downstream location than at the upstream one. However, a consistent discontinuity was observed for the methane and carbon oxides yields just beyond the second membrane panel. The molar flow rate of gas was found to vary along the reactor height, probably as a result of the uneven temperature profile, which can significantly affect the reaction rate as well as the hydrogen permeation rate. The discontinuity in the methane and carbon oxides yields Figs. 12–16 appears to have been due to hydrodynamic effects, above the second membrane. A similar smaller discontinuity appears above the fourth membrane panel as well.

3.3. Hydrogen purity

Hydrogen purities were monitored separately for each membrane panel after each day of experiments. In most cases, the permeate stream was ~99.99% hydrogen. However, for the fourth and sixth membranes, the purity decreased to >99.95% towards the end of the series of experiments. The pure hydrogen production rate depended on the operating conditions and feed flow rates. The highest production rate was 0.39 N m^3 h^{-1} in experiment 9.

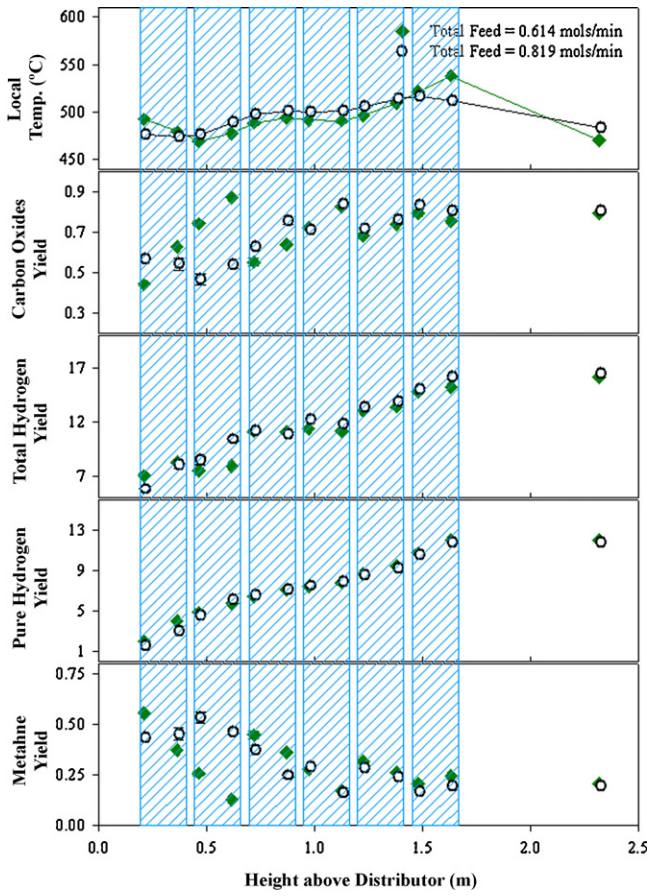

Fig. 16. Experimental yields and temperature for heptane steam reforming at average reactor temperature of 500 °C, pressure 600 kPa, permeate pressure 25 kPa, and steam-to-carbon molar ratio 5.0. Six membrane panels installed.

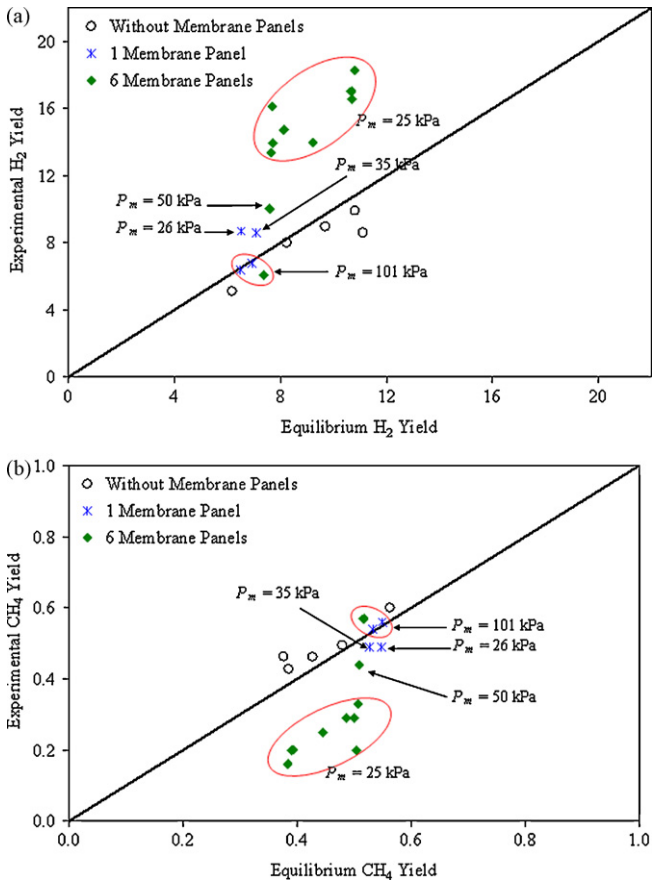

Fig. 17. Parity plot of experimental yields against equilibrium values at local temperatures if there was no hydrogen removal: (a) hydrogen yield and (b) methane yield.

3.4. Discussion

The experimental results show that an FBMR for heptane reforming can be operated at the industrial operating temperatures of naphtha pre-reformers, while achieving hydrogen yields comparable to a second stage steam reformer, which operates at temperatures as high as 850 °C. This is because of the continuous shift of equilibrium limitation as hydrogen is progressively removed. In terms of total hydrogen yield, the FBMR gives the combined performance of a pre-reformer and a reformer. In addition, separate hydrogen purification is not needed, since pure hydrogen is available as a membrane permeate stream. Thus the FBMR combines the function of a pre-reformer, reformer, shift converter, and hydrogen purification section. However, some hydrogen is also lost in the off-gas retentate stream.

Since the FBMR operating temperature is moderate, ~550 °C, catalyst deactivation is minimized, both in terms of carbon formation and sintering. Moderate temperature operation also avoids expensive alloys for high-temperature tubing used in conventional industrial steam reformers.

Heptane conversion exceeded 99% at the lowermost sampling point, and was complete (100%) above that. Except at the very bottom, the FBMR reaction zone sees practically no higher hydrocarbon during steam reforming of heptane. Similar behaviour was observed for steam reforming of propane [53]. Thus the FBMR is flexible in feedstock, similar to what is achieved by addition of a pre-reformer prior to a conventional steam reformer. However, higher hydrocarbon feedstocks require high steam-to-carbon ratios, which can affect the pressure drop in the steam reformer due to variations in volumetric flow rate. Fluidized beds operate with little or no variation of bed pressure drop, although variations of superficial gas velocity may change the hydrodynamic behaviour.

The FBMR process has been widely studied in the past for steam reforming of natural gas. In that case, operation at 550 °C is sufficient to achieve high conversion, equivalent to that at temperatures above 800 °C without membranes [41]. Temperatures >550 °C, although not essential, could improve the hydrogen yield further by enhancing the equilibrium conversion, as well as the hydrogen permeation. The practical temperature limitation arises from the structural integrity of the membranes, which could develop pinholes or cracks. For steam reforming of liquid hydrocarbons like naphtha or its surrogate heptane, as employed in this study, the upper temperature limit is likely to be similar to that for a naphtha pre-reformer.

This study used a model component to emulate steam reforming of naphtha. However, the olefinic components (which must be less than 1% by volume [32]) of naphtha can cause low-temperature catalyst deactivation. To study the feasibility of the FBMR for naphtha steam reforming, the effects of naphthenes and aromatics must also be considered. Nevertheless, the current study provides valuable background information for higher hydrocarbon feedstocks like naphtha, gasoline, kerosene and diesel fuel.

4. Conclusions

Steam reforming of heptane was studied in a fluidized bed membrane reactor, providing insight into the feasibility of FBMR application for hydrogen production from liquid hydrocarbon feedstocks. Experiments were conducted without and with hydrogen

removal. The composition of the reactor gas samples without membranes closely followed the equilibrium values at local temperatures and pressures. The reactor without membranes was equivalent to a pre-reformer for naphtha steam reforming. Effects of hydrogen removal were studied with one and six membrane panels installed. With hydrogen removal through selective membranes, the FBMR provides a compact reformer system, combining the pre-reformer, reformer, shift conversion and hydrogen purification steps into a single unit. The FBMR system is appropriate for steam reforming of higher hydrocarbons, since the temperature limitations of the Pd/Ag membranes closely match the usual pre-reformer temperatures to avoid catalyst deactivation by coking. The FBMR can also accept different hydrocarbon feedstocks. Hydrogen purities as high as 99.99% were achieved from individual membrane panels. The reactor was tested under different operating conditions and flow rates for parametric studies. A pure hydrogen production rate of 0.39 N m^3 h^{-1} was achieved at an average bed temperature of 500 °C, reactor pressure of 600 kPa, permeate pressure of 25 kPa, steam-to-carbon molar ratio of 5 and total feed rate of 0.819 mol min^{-1}. The maximum hydrogen yield was 14.7 moles of pure hydrogen (and 18.5 moles of total hydrogen) per mole of heptane fed, compared with the theoretical maximum of 22.

Acknowledgements

The authors are grateful to Membrane Reactor Technologies, Vancouver for their support during this research. Grants from the Canada Foundation for Innovation (CFI) and the Natural Sciences and Engineering Research Council of Canada (NSERC) are also gratefully acknowledged. One of the authors (M.A.R.) would like to thank NSERC for a doctoral scholarship for two years.

References

[1] J.R. Rostrup-Nielsen, T. Rostrup-Nielsen, CatTech 6 (2002) 150–159.
[2] N. Hallale, F. Liu, Advances in Environmental Research 6 (2001) 81–98.
[3] A. Fonseca, V. Sá, H. Bento, M.L.C. Tavares, G. Pinto, L.A.C.N. Gomes, Journal of Cleaner Production 16 (2008) 1755–1763.
[4] L. Basini, Catalysis Today 106 (2005) 34–40.
[5] B. Johnston, M.C. Mayo, A. Khare, Hydrogen:, Technovation 25 (2005) 569–585.
[6] M. Ball, M. Wietschel, International Journal of Hydrogen Energy 34 (2009) 615–627.
[7] C.J. Winter, International Journal of Hydrogen Energy 30 (2005) 1371–1374.
[8] C.J Winter, International Journal of Hydrogen Energy 30 (2005) 681–685.
[9] C.J. Winter, International Journal of Hydrogen Energy 34 (2009) S1–S52.
[10] B.C.R Ewan, R.W.K. Allen, International Journal of Hydrogen Energy 30 (2005) 809–819.
[11] D.L. Trimm, A.A. Adesina, Praharso, N.W. Cant, Catalysis Today 93–95 (2004) 17–22.
[12] A.K. Avci, Z.I. Onsan, D.L. Trimm, Applied Catalysis A: General 216 (2001) 243–256.
[13] R.K. Kaila, A.O.I. Krause, Studies in Surface Science and Catalysis 147 (2004) 247–252.
[14] http://www.airproducts.com/Products/MerchantGases/HydrogenEnergy/FrequentlyAskedQuestions.htm (accessed 10.11.09).
[15] G. Shumake, J. Small, Hydrocarbon Engineering 11 (2006) 49–52.
[16] J.R. Rostrup-Nielsen, Journal of Catalysis 31 (1973) 173–199.
[17] J.R. Rostrup-Nielsen, Catalysis Today 37 (1997) 225–232.
[18] J.R. Rostrup-Nielsen, P.E. Hojlund-Nielsen, in: J. Oudar, H. Wise (Eds.), Deactivation and Poisoning of Catalysts, Marcel Dekker Inc., New York, 1985, pp. 259–323.
[19] C.H. Bartholomew, Applied Catalysis A: General 212 (2001) 17–60.
[20] J. Sehested, Catalysis Today 111 (2006) 103–110.
[21] J.R. Rostrup-Nielsen, Chemical Engineering Science 50 (1995) 4061–4071.
[22] J.R. Rostrup-Nielsen, J. Sehested, Studies in Surface Science and Catalysis 139 (2001) 1–12.
[23] T.S. Christensen, Applied Catalysis A: General 138 (1996) 285–309.
[24] H. Gunardson, Industrial Gases in Petrochemical Processing, Marcel Dekker, New York, 1998.
[25] J. Gomach, Personal Communication, Sales & Technical Service Engineer, Syngas Catalyst & Technology, Haldor Topsoe, Inc., 2007.
[26] Haldor Topsoe A/S Manual for Topsoe Naphtha Reforming Catalysts, RK-212/RK-202/RK-201.
[27] F. Melo, N. Morlanes, Catalysis Today 107–108 (2005) 458–466.
[28] J.R. Rostrup-Nielsen, in: J.R. Andersen, M. Boudart (Eds.), Catalysis Science and Technology, Springer-Verlag, 1984, pp. 1–117.
[29] J.R. Rostrup-Nielsen, T.S. Christensen, I. Dybkjaer, Studies in Surface Science and Catalysis 113 (1998) 81–95.
[30] Haldor Topsoe A/S Manual: Topsoe Technology for Hydrogen Production (1995).
[31] J.R. Rostrup-Nielsen, Catalysis Today 71 (2002) 243–247.
[32] D.E. Ridler, M.V. Twigg, in: M.V. Twigg (Ed.), Catalyst Handbook, Wolfe Publishing Ltd, London, UK, 1989.
[33] S. Sircar, T.C. Golden, Separation Science and Technology 35 (2000) 667–687.
[34] S.S.E.H. Elnashaie, A.M. Adris, in: J.R. Grace, L.W. Shemilt, M.A. Bergougnou (Eds.), Fluidization VI, Engineering Foundation, 1989, pp. 319–326.
[35] M.A. Soliman, S.S.E.H. Elnashaie, A.S. Al-Ubaid, A. Adris, Chemical Engineering Science 43 (1988) 1801–1806.
[36] A. Brunetti, G. Barbieri, E. Driolia, Chemical Engineering Science 64 (2009) 3448–3454.
[37] Y. Matsumura, J.H. Tong, Topics in Catalysis 51 (2008) 123–132.
[38] A.S. Damle, Journal of Power Sources 186 (2009) 167–177.
[39] Y. Shirasaki, T. Tsuneki, Y. Ota, I. Yasuda, S. Tachibana, H. Nakajima, K. Kobayashi, International Journal of Hydrogen Energy 34 (2009) 4482–4487.
[40] A.M. Adris, C.J. Lim, J.R. Grace, Chemical Engineering Science 49 (1994) 5833–5843.
[41] T. Boyd, J. Grace, C.J. Lim, A.E.M. Adris, International Journal of Chemical Reactor Engineering 3 (2005) A58.
[42] S.A.R.K. Deshmukh, S. Heinrich, L. Morl, M.V.S. Annaland, J.A.M. Kuipers, Chemical Engineering Science 62 (2007) 416–436.
[43] M.A. Rakib, J.R. Grace, S.S.E.H. Elnashaie, C.J. Lim, Y.G. Bolkan, Canadian Journal of Chemical Engineering 86 (2008) 403–412.
[44] Z. Chen, A Novel Circulating Fluidized Bed Membrane Reformer for Efficient Pure Hydrogen Production for Fuel Cells from Higher Hydrocarbons, Auburn University, 2004.
[45] Z. Chen, Y. Yan, S.S.E.H. Elnashaie, AIChE Journal 49 (2003) 1250–1265.
[46] N.A. Darwish, N. Hilal, G. Versteeg, B. Heesink, Fuel 83 (2004) 409–417.
[47] P.B. Tottrup, Applied Catalysis 4 (1982) 377–389.
[48] S.N. Paglieri, J.D. Way, Separation and Purification Methods 31 (2002) 1–169.
[49] S. Uemiya, Separation and Purification Methods 28 (1999) 51–85.
[50] A. Sieverts, G. Zapf, Zeitschrift für Physikalische Chemie 174 (1935) 359–364.
[51] A. Li, J.R. Grace, C.J. Lim, Journal of Membrane Science 306 (2007) 159–165.
[52] Z. Chen, Y.B. Yan, S.S.E.H. Elnashaie, AIChE Journal 49 (2003) 1250–1265.
[53] M.A. Rakib, PhD Dossier: fluidized bed membrane reactor for steam reforming of higher hydrocarbons, University of British Columbia, 2009.